Journal of Nuclear Materials 379 (2008) 80–90

Contents lists available at ScienceDirect

Journal of Nuclear Materials

journal homepage: www.elsevier.com/locate/jnucmat

Corrosion of iron and low alloyed steel within a water saturated brick of clay under anaerobic deep geological disposal conditions: An integrated experiment

F.A. Martin [a,*], C. Bataillon [a], M.L. Schlegel [b]

[a] DEN/DANS/DPC/SCCME/LECA, CEA de Saclay, 91191 Gif sur Yvette, France
[b] DEN/DANS/DPC/SCP/LRSI, CEA de Saclay, 91191 Gif sur Yvette, France

A B S T R A C T

The aim of this study was to determine the corrosion behaviour of iron and low alloyed steels under simulated geological disposal conditions, related to long-term disposal of nuclear wastes in the site of Bure (Meuse-Haute Marne, Champagne, France). The dedicated experiment was a fully integrated set-up: three different bars of material (iron, steel or nickel) have been introduced inside a solid block of clay, which has been saturated with synthetic Bure water and maintained at 90 °C during 8 months. Two types of clay have been tested: first, a compacted MX80 (Wyoming, USA) and second, argilite directly taken from the Bure site (Callovo-Oxfordian). *In situ* electrochemistry has been performed: impedance spectra, chronopotentiometry... The samples have been analysed using a combination of techniques, such as SEM, XRD, EDS, μXAS, μRaman, gravimetry after desquamation. In both cases, the steel or the iron seemed to passivate in contact with the clay. Post-processing of the EIS determined the corrosion rates and the changes in the kinetics have been noticed. The *post mortem* analysis of the corrosion products showed in both cases the presence of an internal layer made of magnetite (Raman, EDX). The external layer was made of partially Ca-substituted siderite ($Fe_{1-x}Ca_xCO_3$), which could play an extra role in the passivation. Moreover, the samples embedded in the Bure argilite presented an intermediate unique layer containing Fe, O, Na and Si. This study suggests the corrosion products started to react with the silica issued from the dissolution of the Bure clay minerals, resulting in clay minerals neo-formation and in corrosion kinetic changes.

1. Introduction

Geological disposal of high-level radioactive waste (HLW) is extensively investigated in several countries to limit long-term exposure of living organisms to radio contamination. According to current designs assessed in France [1], HLW would be stored in stainless steel containers and low-alloy steel overpacks. At the moment, one HLW disposal concept has been chosen: these overpacks in turn would be emplaced directly in the clay host rock of the geological repository, i.e., Callovo-Oxfordian argilite in Bure, France. During the management of the disposal site galleries, it is scheduled that, once the container are put in the overpacks, the drifts are closed as soon as possible. After closure, the time needed to re-saturate the media (immediate surrounding clay) with water and to reach anoxic conditions has been estimated around 30 years [1]. Under the water-saturated, anoxic conditions of the waste repository, and at the temperatures resulting from radioactive decay in the HLW package, iron-clay interaction will result in iron corrosion and clay transformation, ultimately breaking through the overpack [2].

Overpacks are thus intended to remain for more than 1000 years to prevent glass alteration and radionuclide release in the surrounding environment. Moreover, it has been reported that the iron oxides, hydroxides or clay minerals may enhance glass alteration, at least by a mechanism controlled by silica sorption onto these oxides [3,4]. Therefore, an accurate understanding and modelling of metal corrosion, clay transformation, and elemental transport and retention in solid phases is central to predict the fate of the waste overpacks over the next centuries.

Until now, most of the investigations on steel corrosion at the iron-clay interface have focused on smectite destabilization and conversion to new minerals [2,5–10]. Thermochemical models [5,6] predicted that clay corrosion in the presence of metallic Fe would lead to the formation of Fe-rich clay minerals. Debruyn et al. [11] show that corrosion of low alloy steel in contact with Boom clay, at 90 °C, produces mainly magnetite (Fe_3O_4) and hematite (Fe_2O_3). SiO_2 is also noticed into the corrosion layers. Other studies focused more on the role of clay in the corrosion process [12,13]. The clay minerals involved in the corrosion processes are mainly the swelling layers (montmorillonite, nontronite, beidellite).

* Corresponding author. Tel.: +33 (0)16908 4886; fax: +33 (0)16908 1586.
E-mail address: frantz.martin@cea.fr (F.A. Martin).

0022-3115/$ - see front matter © 2008 Elsevier B.V. All rights reserved.
doi:10.1016/j.jnucmat.2008.06.021

At low temperature (up to 90 °C) and basic conditions, Fe-rich phases from the serpentine group are formed (berthierine, cronstedtite or odinite) all together with an amorphous reactive gel, in which nucleation proceeds [10,13].

Up to now, no real-time kinetic study on the corrosion process under such geological conditions (callovo-Oxfordian clay, anaerobic environment, $T = 90$ °C) has been carried out, neither on the observation of the corrosion rate evolution with time for long testing periods, nor on the intensive changes in the corrosion products with time. This gap in our knowledge was mainly due to the difficulty to reproduce the geological conditions at the laboratory scale. To better mimic the interfacial geometry of the canister-clay contact, integrated electrochemical experiments were designed, in which the steel corrosion would be evaluated by electrochemical measurements [14]. Complementary to these *in situ*, real-time measurements, the reaction end-products could be characterized by microscopic techniques at the scale of the corrosion layers (SEM-EDX [15], μRaman [16] or XANES [17] for instance).

This paper aims at detailing this dedicated integrated experiment, and mainly focuses on the corrosion processes and mechanisms involved during the tests. These latter were the first real laboratory tests to reproduce at best the underground conditions of the repository site of Bure, France. It would permit to monitor *in situ* the evolution of the corrosion kinetics, to identify the corrosion products and ideally to assign a structural modification in the corrosion products to these kinetic changes. These post-mortem characterisations are beyond the scope of this paper but are fully reported by Schlegel et al. [18] and will be greatly referred to in last section. These findings place constraint on the models of iron-clay interaction in the French nuclear waste repository.

2. Experimental

2.1. Materials and set-up

Two sets of experiments, baptised Arcorr2004 and Arcorr2005, have been performed. Both experiments used the same original set-up, but tested materials in two types of clay. The material tested was a low alloyed steel (1050) for both experiments, as well as pure iron for Arcorr2005. Arcorr2004 was performed in bentonite type MX80 compacted clay at dry density: 1.8 [19,20], whereas Arcorr2005 used Bure site (France) argilite rocky clay [21,22], extracted at a depth of 495 meters below earth level (mineralogical compositions given in Tables 1 and 2). The use of MX80 compacted clay was necessary for comparison with the Bure site clay behaviour, and was taken as a reference (model clay). For these experimental sets, the clay used was machined into a cube, in which cylindrical holes were made in order to fit in the steel samples.

In order to reconstitute at best the actual underground conditions of the site of Bure, synthetic water has been prepared according to former analysis of Bure water [23] (composition is given in Table 3). This solution has been conditioned by a gaseous cover, made of (0.1% H_2, 22% CO_2 in Ar) in order to fix the pH of the solution to 7.3 at room temperature. The autoclave was heat controlled at 90 °C. An overpressure of about 44 bars of He has been added in the autoclave to push the synthetic solution in the confinement cell containing the clay cube and the samples.

The confinement cell itself was made of stainless steel structure with Ni inset so that the brick of clay was only in contact with Ni, in order to avoid any contamination by Cr or Fe. A sketch of the complete set-up is represented on Fig. 1.

At the start of the experiments, the brick of clay is saturated with the conditioned synthetic water.

Table 1
Mineralogical composition of MX80 clay (from [19,20])

Phase	Amount (wt%)	Chemical formula
Montmorillonite	71–76	$(Si_{3.96}Al_{0.04})(Al_{1.52}Mg_{0.26}Fe^{III}_{0.17})Na_{0.18}Ca_{0.11}O_{10}(OH)_2$
Phlogopite 1M	2–3.8	$Mg_3Si_3AlO_{10}(OH)_2K$
Pyrite	0.5	FeS
Calcite	0.3–1.4	$CaCO_3$
Anatase	0.1	TiO_2
Plagioclases	3.1	Na Al Si_3O_8
Feldspath K	1.1	K Al Si_3O_8
Phosphate	0.3	Ca Na PO_4
Quartz + Cristobalite	5–6	SiO_2
Molecular water	10.8	H_2O

Table 2
Simplified mineralogical composition of the Callovo-Oxfordian clay extracted from the Bure site (from [21,22])

Phase	Amount (wt%)	Chemical formula
Illite	35	$K_{0.6}Mg_{0.25}Al_{2..3}Si_{3.5}O_{10}(OH)_2$
Quartz	25	SiO_2
Calcite	17	$CaCO_3$
Montmorillonite-Na,Ca	15	$(Ca_{0.167},Na_{0.33})Mg_{0.33}Al_{1.67}Si_4O_{10}(OH)_2$
Dolomite	3.5	$MgCa(CO_3)_2$
Kaolinite	1.3	$Al_2Si_2O_5(OH)_4$
Feldspath K	1.3	K Al Si_3O_8
Albite	1.3	$NaAlSi_3O_8$
Pyrite	1	FeS
Goethite	0.4	Fe_2O_3

2.2. Electrochemical monitoring

The electrochemical measures have been realised with a three-electrode set-up. It consisted in a three electrodes cell:

- A nickel (Arcorr2004) or 1050 (Arcorr2005) electrode is kept in the clay brick and acts as a pseudo reference electrode for the potential measurement.
- The cell walls play the role of counter electrode.
- The two samples cast into the clay brick constitute the working electrodes.

In Arcorr2004, the working electrodes were two electrodes of 1050 steel surrounding a nickel electrode. In Arcorr2005, the nickel electrode was replaced by a pure iron electrode, in order to perform the analysis after the experiment (no perlitic phase).

The electrochemical impedance spectra have been obtained at free corrosion potential, thanks to a SOLARTRON rack, including a signal frequency response generator/analyser (1250 type), HP 362 computer monitored, coupled to two 1286-type potentiostats. This specific set-up permitted to perform impedance measures down to frequencies as low as 20 μHz. In this study, it will be assumed that the proportionality between the corrosion current and the transfer conductance remains unchanged during the entire test.

2.3. Structural analysis

The surface was observed with a set of spectroscopic and microscopic techniques. Of these, micro-X-ray fluorescence and micro-X-ray absorption were used first, and micro-X-ray diffraction was used last. Thus, the sample may have undergone some transformation between successive characterizations.

The surface was first mapped with an optical microscope (Olympus BX51M) to identify the major interfacial units. Samples were then imaged with a scanning electron microscope (JEOL

Table 3
Chemical composition of the synthetic solution representative of Bure argilite interstitial water (from [23])

	Cations				Anions			
	Na^+	K^+	Ca^{2+}	Mg^{2+}	Si	Cl^-	SO_4^{2-}	HCO_3^-
mmol/kg	7.3	2.5	8.6	6.5	0.1	35	1.7	1.6
ppm	167.8	97.8	344.7	158.0	2.81	1241	163.3	97.6
meq/kg	7.30	2.50	17.20	13.00		−35.00	−3.40	−1.60
meq/kg	40.00					−40.00		

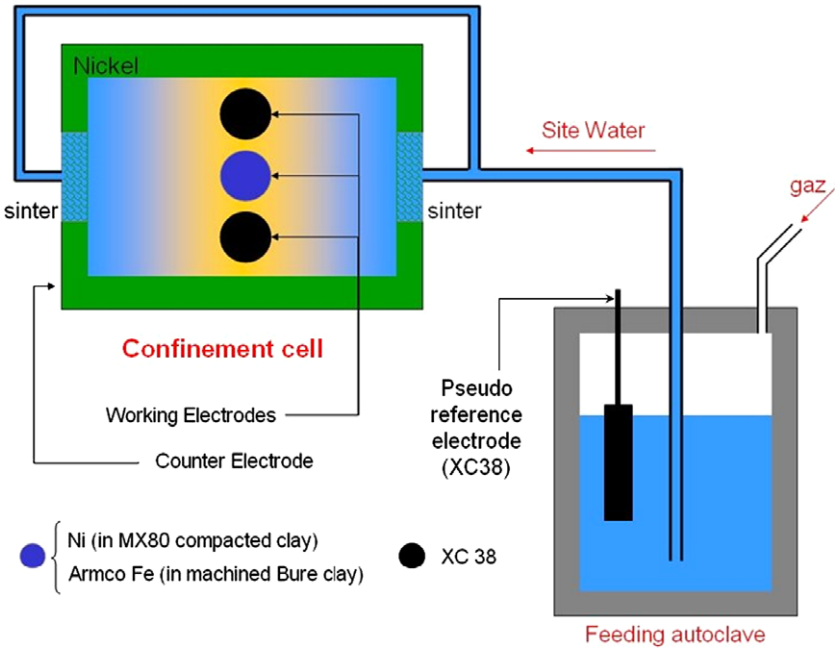

Fig. 1. General scheme of the set-up. The electrode in the feeding autoclave is either in Ni (for Arcorr2004) or 1050 steel (for Arcorr2005) and plays the role of reference for the potentials. Inside the confinement cell, three working electrodes have been positioned: two 1050 electrodes (top and bottom) and one central electrode either made of Ni or made of Fe.

JSM7000-F) equipped with a field emission gun. The electrons were accelerated to 10 kV to minimize the electron penetration depth while exciting the Fe Kα line. Surfaces were coated with a thin carbon film. Energy-dispersive X-ray (EDX) analysis was performed using a Si(Li) detector (Oxford Instruments), equipped with a thin Be window to detect and quantify oxygen with a good accuracy. The EDX analyses were collected and processed using the Spirit system (Synergy 4 – PGT).

3. Characterisation of the clayey electrolytes

The basic work has been done mainly on the compacted MX80 clay, assuming the overall conclusions could be generalised to any clay of the same type. In the case of the Arcorr04 experiment (MX80 clay), the confinement cell contains a brick of clay in which are inserted three rods (electrodes): two in 1050 carbon steel and one in nickel. The latter is inserted in the central part of the brick. On the other hand, another nickel electrode is placed inside the feeding autoclave. The goal here was to study the electrochemical reactivity of compacted clay saturated with the synthetic solution.

3.1. Electrolyte resistance

The electrolyte resistance R_e has been measured by EIS. The values were extracted from the EIS spectra used for the corrosion monitoring. This resistance R_e is the sum of two terms: the apparent ionic resistance R_a of the clay saturated by synthetic water and the ionic resistance R_s of the synthetic water present inside the nickel sinter, the tube linking the confinement cell and the autoclave, then the feeding autoclave. Fortunately the R_s part is common to the three electrodes inserted in the confinement cell. Former measures of the apparent ionic resistance of the synthetic water present inside the feeding autoclave indicated variations with time (2–5 Ω). Therefore, the variations of R_e can not only be attributed to clay effects. Fig. 2 show the evolution of R_e seen by the samples in compacted water-saturated MX80 clay and in water-saturated Callovo-Oxfordian argilite respectively. Ondulations of R_e with time are noticed, but no conclusion could be drawn from them. However, the difference between two samples under the same conditions (see Fig. 2(a) and (b)) tend to show that these variations might mostly be linked to apparent ionic resistance variations of the clay at the vicinity of the samples. This result would thus confirm that the brick of clay present local heterogeneities, which could be induced by hydrogen release associated with corrosion process.

3.2. Cyclic voltammetry

In Fig. 3, two raw voltamperograms obtained at a scanning rate of 10 mV/s on the same range of potentials are presented. One concerns the Ni electrode immersed in the autoclave, whereas the

other concerns the Ni electrode inserted in the solution saturated compacted MX80 clay. In the autoclave, the nickel presents a cathodic branch, corresponding to water or proton reduction, and an anodic branch, related to hydrogen or water oxidation. In the brick of clay, one anodic peak and one cathodic peak are revealed. Actually, the current density is much higher when the electrode is inserted in the compacted clay than in the solution. This shows a specific electrochemical activity inside the clay exists. In other terms, it exists in clay, or clay 'produces' by self-degradation, an electro-active species of a Red/Ox couple, which does not exist in the synthetic Bure water. Moreover, the cathodic peak is only observed when the anodic peak is first observed, which means the electro-active species is in its reduced state.

According to the mineralogical composition of MX80 clay, two sources of electro-active species could be identified: pyrite (sulphides) or montmorillonite (Fe ions). On the one hand, the dissolution of pyrite would give sulphides, which could, considering the pH and the Pourbaix diagrams [24], get oxidised into sulphur then in sulphate ions. Since the synthetic solution already contains sulphates, which do not seem to be reduced during the linear voltage scan, the probability that sulphides are the electro-active species is low. On the other hand, dissolution or destabilisation of the montmorillonite could lead to the injection of Fe^{3+} in the interstitial water of clay. In presence of a subsequent amount of dissolved hydrogen, these Fe^{3+} cations could be chemically reduced into Fe^{2+}. Then, on the nickel during voltammetry these Fe^{2+} cations could be electrochemically oxidised into Fe^{3+} then once more reduced into Fe^{2+}.

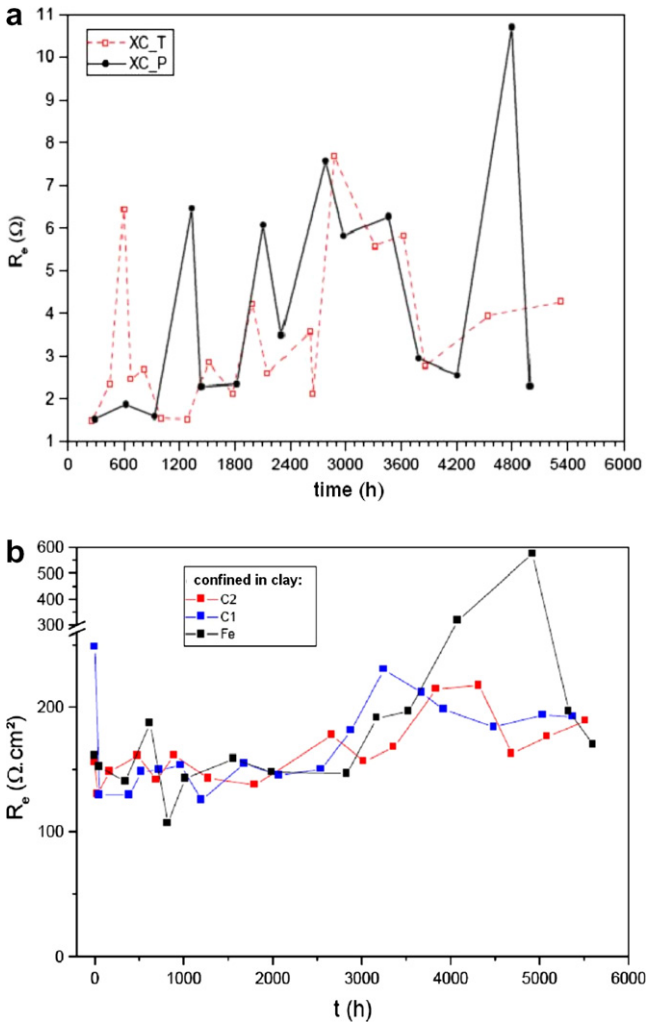

Fig. 2. (a) Time evolution of the value of the apparent resistance of the media seen by the steel electrodes embedded in the brick of MX80 clay at 90 °C and (b) Time evolution of the value of the apparent resistance of the media seen by the steel electrodes embedded in the brick of argilite clay at 90 °C.

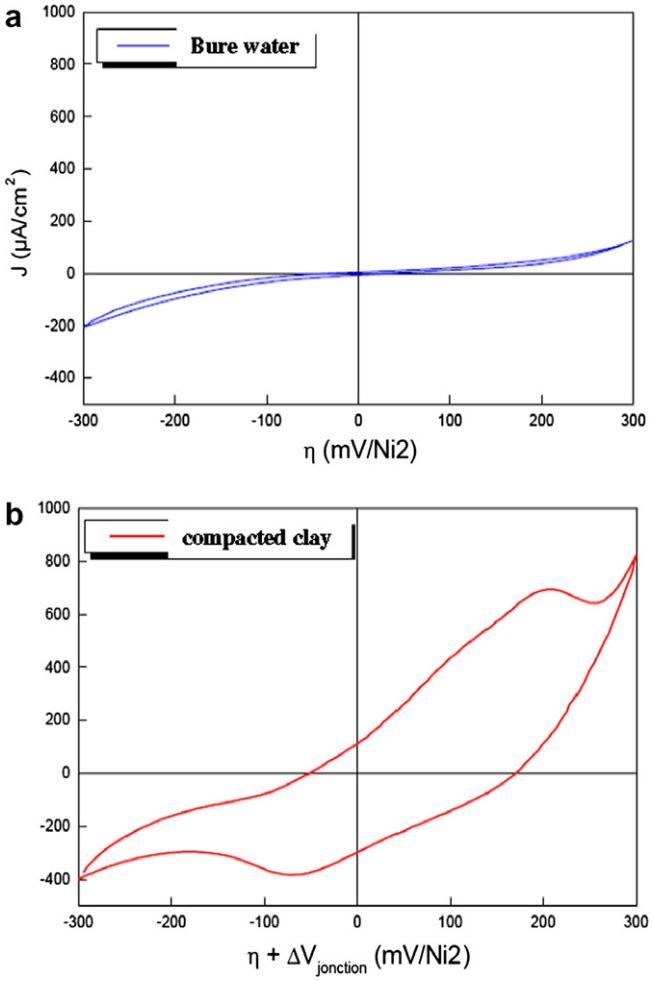

Fig. 3. Voltammograms obtained at 10 mV/s scan rate on Ni electrodes. Top, Ni electrode simply immersed in synthetic Bure water at 90 °C (inside the feeding autoclave); Bottom, Ni electrode inserted in MX80 compacted clay saturated with synthetic water at 90 °C (confinement cell).

Nevertheless, it still remains impossible to differentiate which of the two potential electro-active species is effectively the one which is responsible for the establishing of the anodic and cathodic peaks. The introduction of one of the two Red/Ox couples into the synthetic solution would thus be the only way to find out, but it was beyond the scope of this study.

4. 1050 steel – MX80 compacted clay interactions

4.1. In situ electrochemical monitoring of 1050 steel corrosion in compacted MX80

In order to follow the process of corrosion of the 1050 steel in compacted clay saturated by synthetic water, chronopotentiometry and impedance spectroscopy have been used. Linear scan voltamperometry has not been used because this technique highly disturbs the corrosion process. The two electrodes are situated above and below the nickel rod, and named XC_T and XC_P, respectively. The comparison of the results permits to evaluate the repeatability of the experiment.

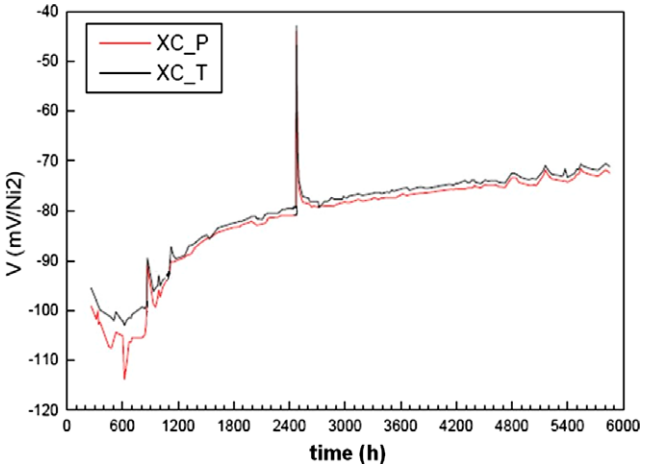

Fig. 4. Chronopotentiometric plot of the evolution of the potential of the two 1050 steel electrodes in the brick of MX80 clay compared to the Ni electrode inside the autoclave (taken as reference).

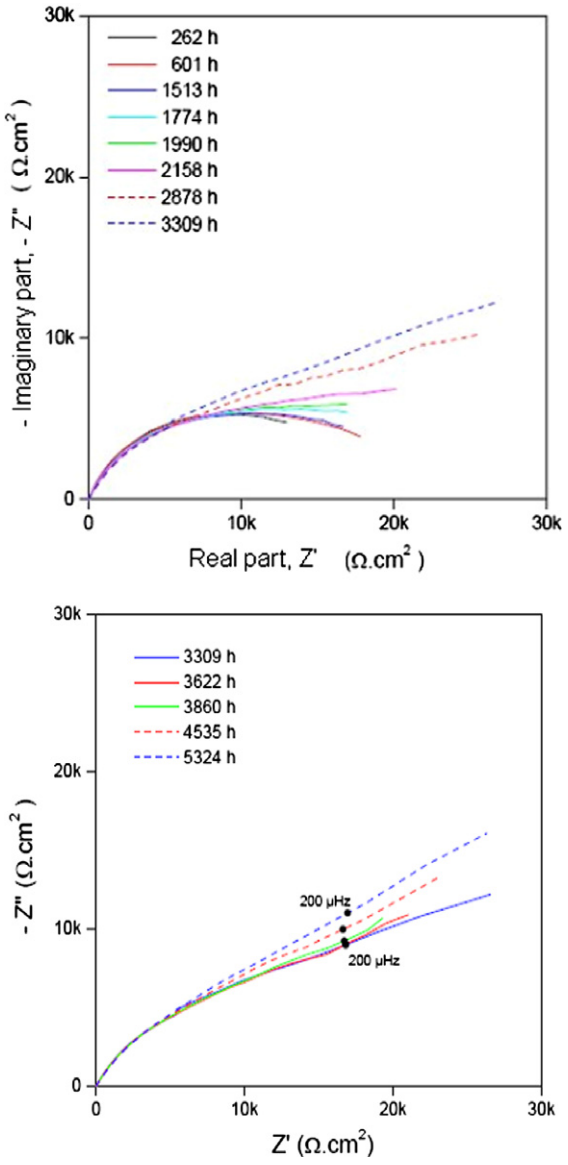

Fig. 5. Evolution of the electrochemical impedance spectra in Nyquist representation of the XC_T low alloyed steel sample with the duration of the experiment in compacted MX80 clay (saturated with synthetic water at 90 °C).

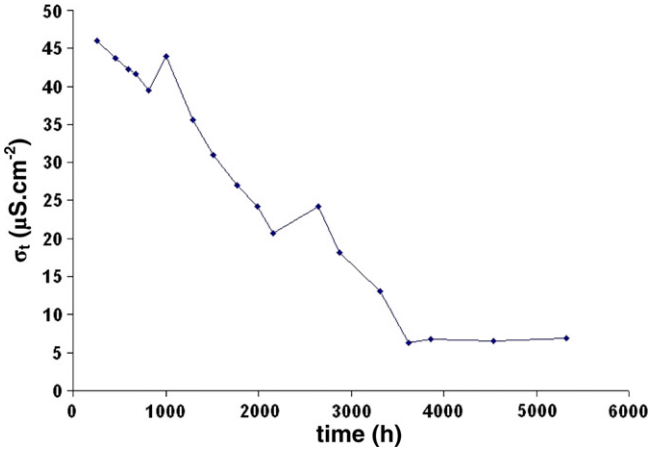

Fig. 6. Evolution of the transfer conductance as function of the duration of the test for the sample XC_T, in compacted MX80 clay.

The chronopotentiometry shows mainly that the two steel electrodes evolve similarly and almost fit each other, which indicate a good reproducibility of the experiment. Moreover, their potential (compared to the Ni electrode) increases and tends towards an asymptote at infinite times, which highlights a slight ennoblement of the material (Fig. 4).

Concerning the impedance spectra, attention has been paid on their evolution with the duration of the experiment on a qualitative point of view. In both cases, the Ni electrode was taken as the pseudo potential reference electrode. The results obtained on the XC_T and XC_P samples are very similar, and only the spectra of the XC_T sample are presented in Fig. 5. In both cases, two distinct periods of time have been observed. For short times ($t < 2000$ h), the impedance spectra look like a flattened capacitive loop. For long times ($t > 3000$ h), the impedance spectra seem to behave like a constant phase element (CPE), even in the very low frequencies domain ($f < 0.2$ mHz). This CPE is defined:

$$C(\omega) = C_\infty + \Delta C(i\omega)^n = \frac{1}{i\omega[Z(\omega) - R_e]}, \quad (1)$$

where n is a real number comprised between 0 and 1 and C_∞ a pure capacity.

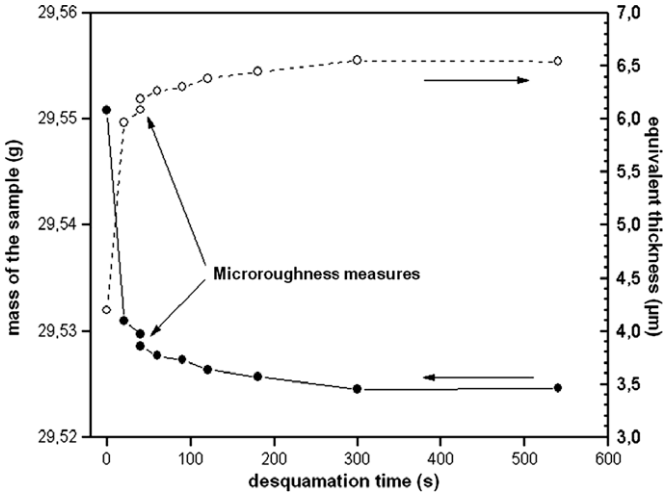

Fig. 7. Desquamation plot for the sample XC_T. The evolution with desquamation time of the sample mass is plot (left), as well as the corresponding steel thickness loss (right).

The evolution of the impedance spectra obtained with sample XC_T is quite monotonous. For short times, the observed capacitive loop increases it diameter with time and 'opens' to reach the appearance of a low frequency CPE from 2158 h. For longer times, the real part of the CPE is almost constant whereas the imaginary part increases regularly. This evolution shows qualitatively a change in the corrosion kinetics, with a trend to a slow down of the corrosion process. Nevertheless, post processing on these impedance spectra permitted to extract the transfer resistance (R_t) values. As long as the spectra were capacitive loops, R_t was an easy data to access. The difficulty came with the determination of R_t when CPE dominated the spectra. As detailed by Bataillon et al. [25], the value of R_t can be extracted thanks to log–log appropriate plots in the HF range, then parameters can be corrected for a best fit in linear Nyquist plots. It appears that it was in general possible to fit correctly the experimental spectra, which allowed us to extract the corresponding R_t values. The application of Butler–Volmer equation to the system in impedance spectroscopy gives the linear relationship between the corrosion current and the transfer conductance σ_t ($\sigma_t = \frac{1}{R_t}$), as given:

$$j_{corr} = \frac{RT}{F}\lambda\sigma_t \tag{2}$$

with F a Faraday (96485 C), and λ a constant defined by $\lambda = \frac{1}{(\alpha_a n_{Fe} + \alpha_c n_c)}$, where α_a and α_c are the Butler–Volmer coefficients, n_{Fe} the iron oxidation valence (i.e., 2 or 3) and n_c the number of electrons exchanged in the cathodic reaction (i.e., 1 according to Butler–Volmer or Volmer–Heyrovsky).

Considering the case of dissolution of pure iron, the corrosion rate could thus be deduced:

$$v_{corr} = \frac{RT}{F}\lambda\frac{M_{Fe}}{n_{Fe}\rho F}\sigma_t \tag{3}$$

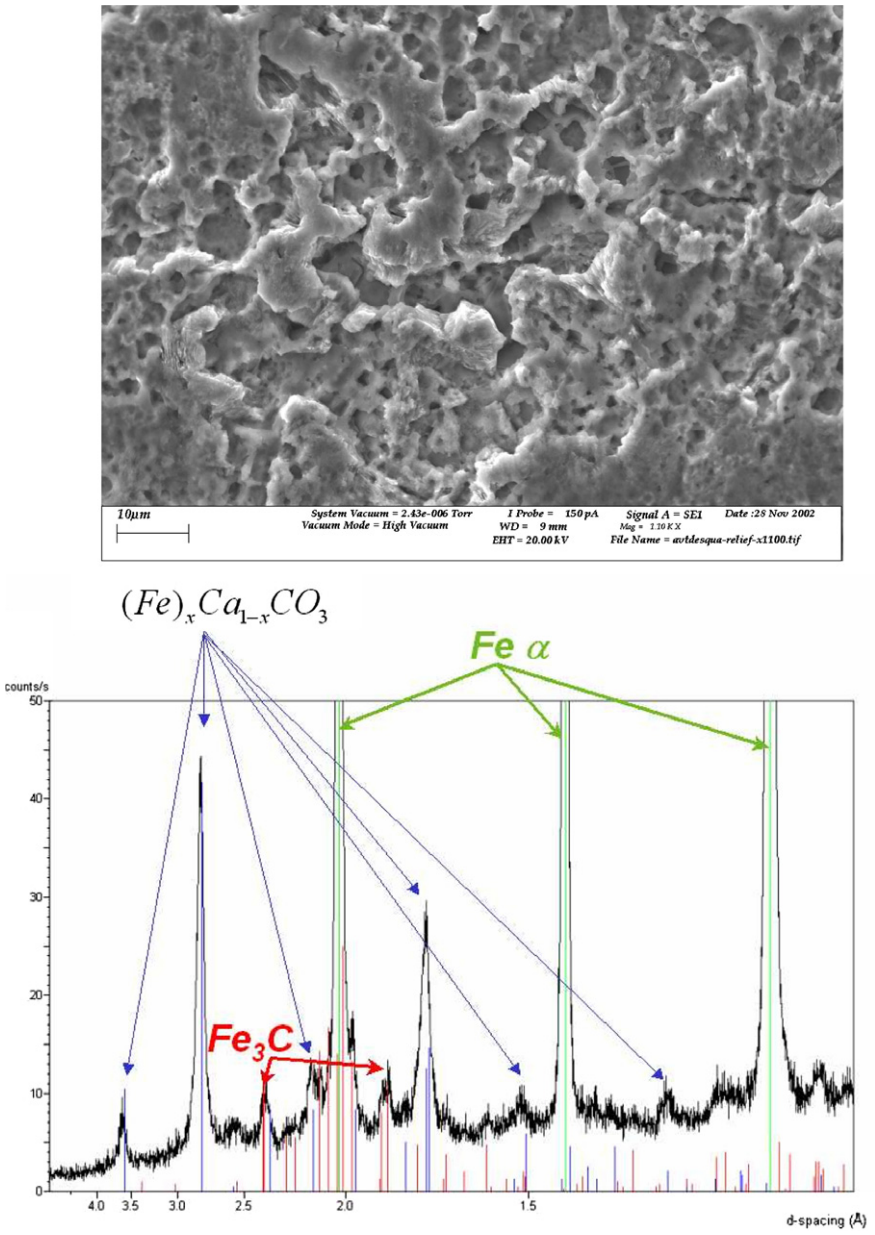

Fig. 8. SEM micrograph of the surface of XC_T sample after the test but before desquamation (top) and the corresponding XRD spectrum (bottom). The Ca-substituted siderite layer is continuous and looks compressed. Fe_3C and ferrite are still observable: the layer is thin.

with M_{Fe} and ρ the atomic weight and density of pure iron, respectively.

Eq. (3) shows clearly the linear relationship between the instantaneous (reliable only at the moment when the impedance spectrum has been acquired) corrosion rate and the transfer conductance. Therefore, plotting σ_t versus time would show the trend of the instantaneous corrosion rate during the whole experiment. Fig. 6 gathers the evolution of σ_t with time for the sample XC_T. Since the fit technique is qualitative, the error margin is not negligible (20%), which could explain some data a little out of the main trend line. The corrosion rate thus decreased with time and seems to tend towards an asymptote for long times, indicating the system reached a stationary regime. However, in the focus of this study, to quantify the corrosion rate was a necessity, therefore, to assign a value to the constant λ. Gravimetry measurements might satisfy this request.

4.2. Gravimetry measurements: determination of the mean corrosion rate

The desquamation (pickling) of the samples XC_T and XC_P has been carried out in a solution containing 50% hydrochloric acid in volume in deionised water and 5 g/L of hexamethylenetetramine. Focus has been made on XC_T sample (for correlation with EIS measures). The evolutions of the weight of XC_T sample as well as steel thickness loss of XC_T sample with desquamation time are represented in Fig. 7. The thickness is deduced from weight thanks to geometrical considerations and the estimation of the corrosion products density as 5 g/cm^3. The total loss of thickness during the 6000 h of the experiment was estimated to 6.44 ± 0.04 μm. For this sample, the uncertainty on the measure was estimated to 0.1 μm. This loss corresponds to a mean corrosion rate of 9.5 μm per year.

4.3. Corrosion products

The nature of the external corrosion products has been determined on XC_T sample thanks to SEM, EDS then XRD analysis prior to desquamation. The SEM examination of the corroded sample revealed a relatively homogeneous surface. The EDS spectrum recorded on different areas of the surface confirmed this homogeneity. The surface of the corroded steel was covered by a layer containing carbon, oxygen and iron as major elements and calcium, manganese, chromium, silicon and aluminium as minor elements. On some areas, the Si and Al peaks were bigger. These areas exhibited some localised sediments, which seemed to be clay particles that had not been removed during the ultrasonic bath.

XRD analysis of the corroded surface showed the surface was covered by a mixed iron-calcium carbonate layer (Fig. 8). Indeed, the peaks corresponding to this carbonate were slightly shifted towards low displacements compared to the siderite peaks. It means a substitution of an iron cation by a higher ionic radius cation occurred. According to the EDS spectra, this substitution cation was calcium, thus the carbonate could be written as $(Fe)_x$-Ca_{1-xCO3}. The other peaks of the XRD spectra were assigned to α-ferrite and Fe_3C. SEM observations of the interface exhibited a homogeneous surface, quite coarse but compact and continuous (Fig. 8).

4.4. Discussion

The *in situ* EIS monitoring of corrosion of the 1050 steel in compacted water-saturated MX80 clay was successfully carried out and it appeared that on the duration of the test, the corrosion rate decreased monotonously, with an average corrosion rate of 9.5 μm/year. However, the knowledge needed in such long term prediction studies is the effective instantaneous corrosion rate, in

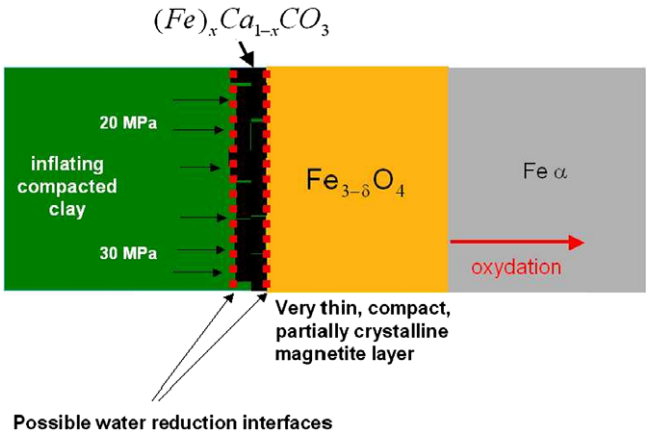

Fig. 9. Sketch of the interfaces observed and of the interfacial reactions, as deduced from the study. At first Fe oxidises into magnetite. At the surface of magnetite, water is reduced and Fe(II) is released in the pore solution, interacting with clay. Then calcium-substituted siderite is formed at the magnetite external surface and accumulates there. After a while the pressure due to swelling of the surrounding clay impacts on the circulation of species and blocks the pores of the siderite. The magnetite surface is thus no more attainable for water reduction, which finally occurs at the newly formed clay/calcium-substituted siderite interface.

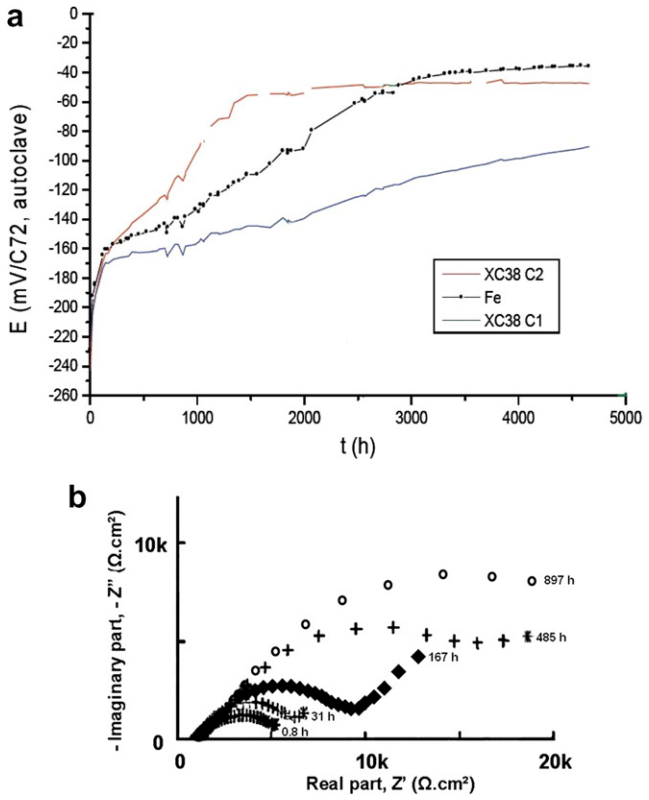

Fig. 10. (a) Chronopotentiometric plot of the evolution of the potential of the three electrodes (two 1050 and one pure Fe) in the brick of Callovo-Oxfordian clay compared to the 1050 electrode inside the autoclave (taken as reference) and (b) Evolution of the electrochemical impedance spectra in Nyquist representation of the 1050_C1 low alloyed steel sample with the duration of the experiment in Bure argilite (saturated with synthetic water at 90 °C). After 700 h, the very low frequency part has overwhelmed the figure: the kinetics is controlled by very slow processes, like species diffusion.

order to give a trend and extrapolate for longer times. As seen before, the constant λ has to be determined.

In fact, it is also possible to calculate the mean corrosion rate over the duration of the experiment by using the instantaneous corrosion rates described in the former section. It gives:

$$v_{\mathrm{corr}}^{\mathrm{average}} = \lambda \frac{RT}{F\Delta t} \Sigma_{i=1}^{n} \left[\frac{\sigma_t^{\mathrm{inst}}(t_{i-1}) + \sigma_t^{\mathrm{inst}}(t_i)}{2} (t_i - t_{i-1}) \right]. \quad (4)$$

Equalising Eq. (4) to 9.5 μm/year gives λ, which in turn can be reintroduced in equations of the (3) type and finally give the values of the instantaneous corrosion rates deduced from the EIS. The final stationary state corrosion rate was, therefore, estimated to 3 μm/year.

The 1050 steel thus tended to passivate under the experimental conditions, even if this passivation seems far less efficient than the one of stainless steels.

Concerning the surface/corrosion products analysis, it appeared that the surface was covered by a very thin layer of magnetite, itself covered by a thin homogeneous calcium substituted siderite layer. From these observations, a corrosion mechanism was suggested (see Fig. 9): the steel oxidised, creating a $Fe_{3-\delta}O_4$ homogeneous thin layer, oxidation of Fe taking place at the magnetite/metal interface. The magnetite layer generally acts as a passive layer for higher thicknesses and could not be alone responsible for the 'passivation' of the sample with time in the compacted water-saturated clay. At the outer interface of magnetite, it is suggested that water is reduced and that iron Fe^{2+} cations are released, forming siderite. This layer of siderite would progressively get substituted with calcium cations, forming the observed outer layer. Since this kind of clay is swelling, another phenomenon could also occur: in the first steps of corrosion, the reduction interface could be the outer interface of magnetite, then after a while, the swelling effect of MX80 might block and fill all the porosities of this calcium substituted siderite and water reduction would thus occur at the outer surface of the latter. This change in the location of the reduction of water could be relevant with the changes observed on the EIS spectra between short times and long times, which was associated to a change in the corrosion kinetics (see above).

5. 1050 steel – Bure clay interactions

5.1. In situ electrochemical monitoring of 1050 steel corrosion in Bure argillite

As in MX80 compacted clay, three electrodes were inserted into the brick of callovo-Oxfordian argilite: one central pure iron rod, two 1050 steel rods, XC38 C2 and XC38 C1, above and below respectively. In the mean time, two 1050 steel electrodes were plunged in the feeding autoclave, for comparison.

Chronopotentiometry has been carried out as a control measure, and the curves obtained for the two steel and the pure iron electrode inside the argilite is presented in Fig. 10(a)). The evolution of the potential with time could be split in 3 phases: first, the potentials increase quickly towards anodic values during the first 150 h of the experiment. This phase is relevant with the saturation of the brick in synthetic Bure water. For times in the range [150; 2000] hours (depending on the sample considered), a transition is clearly evidenced. For longer times, the evolution of the potential becomes linear with a small slope, all the curves tending towards the same asymptote. This behaviour reminds us the former experiment in MX80 clay: a progressive and individual ennoblement of the materials tested is observed. The delays observed between the samples could be attributed to the fact that the clay is natural, though not homogeneous.

On an EIS point of view, the three samples seemed to behave similarly. In the Nyquist plan, the spectra obtained were indeed much alike and their shape could be described as follow (see Fig. 10(b)): at high frequencies (HF), the spectrum started with a series of point aligned on a straight line inclined of 45° in the Nyquist plan (diffusion processes). At medium frequencies (MF), the impedance was described by a flattened semi-circle, which diameter increased with time. This MF part gives information about the metal/layer interface. At low (or very low) frequencies (LF), the diagram is again made of aligned spots on a straight line inclined of 45°. The LF part of the plots could concern solid state diffusion in magnetite or in outer corrosion products.

Moreover, the characteristic frequencies of the processes decreased highly with the duration of the experiment: the frequency

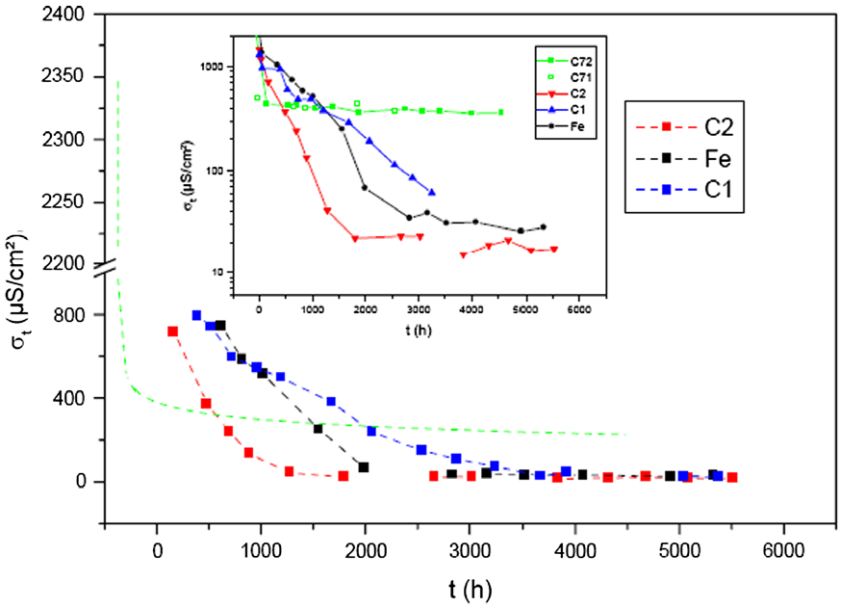

Fig. 11. Evolution of the transfer conductance as function of the duration of the test for the three samples (1050 and Fe) embedded in the brick of Bure argillite. The inset is a log representation to enhance the contrast for low σ_t values in comparison with the values obtained for 1050 in the autoclave (free solution, dashed line called C71 or C72).

at the summit of the semi-circle passed from 631 mHz to 6.3 mHz in almost 700 h. Consequently, the more time passes by, the bigger the proportion of the corrosion semi-circle attributed to LF becomes. This shows an increase of the contribution of diffusion processes to R_t, so to v_{corr} with time, leading to a total control of the corrosion kinetics by diffusion aspects. It seems that after 8 month of test, the corrosion of iron confined in anaerobic water saturated argilite might be limited by diffusion inside the corrosion products situated at the external interface of the material. This observation tends to confirm a change of regime in the corrosion kinetics, correlated to the chronopotentiometry plots.

Nevertheless, it was assumed that σ_t could be deduced with low error margins from the semi-circle part only. Thus post-processing on the EIS spectra has provided the transfer conductance values σ_t, which have been plotted versus time in Fig. 11. As scheduled, the corrosion rate decreased, highlighting a passivation process. It means the intimate contact of the material with the water-saturated brick of argilite protected the material against corrosion effects.

Following the same procedure as above for MX80 clay, gravimetry measurements were necessary to link σ_t to the corrosion rate.

5.2. Gravimetry

Unfortunately, acidic solution was not able to get rid of the totality of the covering corrosion products and/or transformed clay layers, preventing any gravimetric measure.

5.3. Corrosion products

After the desquamation tries, the samples were only partially cleared of the corrosion products. In fact, three different regions could be distinguished: one black metallic-like surface (black zone), one median heterogeneous layer rust-coloured and one external layer (thicker), where a grey product cover remained stuck on the surface.

In fact, these different areas have been roughly examined before further investigations, thanks to SEM, EDS and XRD. Two spots have been studied: the first one localised on the black zone and the second one on the external layer. In the black zone, mainly ferrite (α-Fe), siderite ($FeCO_3$) and some cementite (Fe_3C) have been evidenced. Peak shifts on the spectra of siderite would suggest that it might be calcium substituted siderite. The study of the external layer showed mainly quartz (SiO_2) and calcite ($CaCO_3$), as well as some silicates like $Fe_{0.24}Mg_{0.76}SiO_3$ or Ca_2SiO_4, $_{0.35}H_2O$, which is relevant with transformed clay. For sure, the metallic surface is covered by a magnetite thin film, itself covered by calcium substituted siderite, like in the study with MX80 clay, then with more or less transformed clay minerals (see Fig. 12). Nevertheless, it did not explain the different behaviour of the corrosion product layers in the desquamation bath. Would it be possible that another compound was created in the argilite, which would interact between the siderite and the transformed clay so that it did not dissolve in HCl? Further analyses were thus necessary.

Due to the apparent complexity of the layers formed on the steel samples, and taking into account that the pure iron electrode remained untouched, plus the fact it behaved like 1050 C1 and 1050 C2 during the EIS monitoring, full analysis have been done on this pure iron rod. In order to minimize the disturbance of the Fe sample and its surroundings (corrosion products + clay minerals), it has been impregnated with epoxy resin, then cut and polished.

SEM, EDX, μ-Raman and XANES have been performed on cross-sections of the iron sample. The results of these analyses have been published by Schlegel et al. [18].

5.4. Discussion

The electrochemical measures showed two main features: first, that the saturation of the argilite brick is quick (150 h), like in the case of MX80 clay resaturation (100 h) and second, that the corrosion process of the samples can be split in two stages. At first, a protective layer is forming (decrease of v_{corr}), second a limiting process occurs, ruled by the diffusion of species inside this protective layer.

No corrosion rate could be evaluated. However, the present study just showed the corrosion products were not entirely identical in MX80 and in Callovo-Oxfordian clay, even if the external

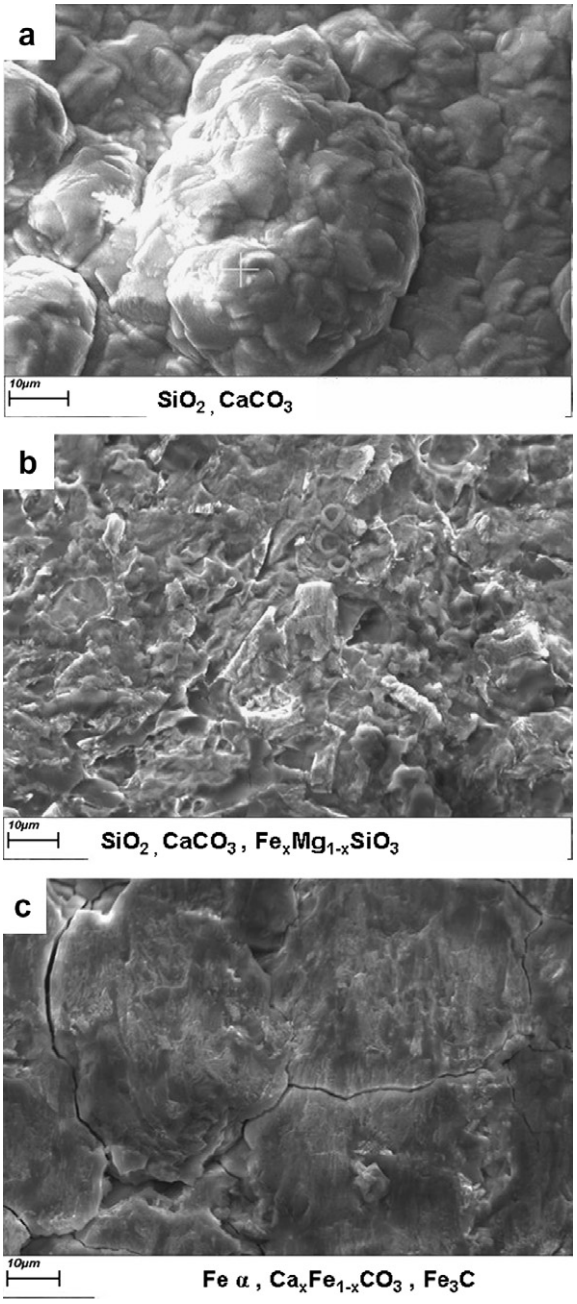

Fig. 12. SEM micrographs of the different areas mentioned after desquamation tries and their associated main components, found by EDS. (a) external layer mainly constituted of SiO_2 and $CaCO_3$, (b) median layer made of SiO_2, $CaCO_3$ and other compounds like $Fe_xMg_{1-x}SiO_3$ and (c) black zone, essentially made of ferrite, siderite and cementite: the former oxide grain boundaries are still visible.

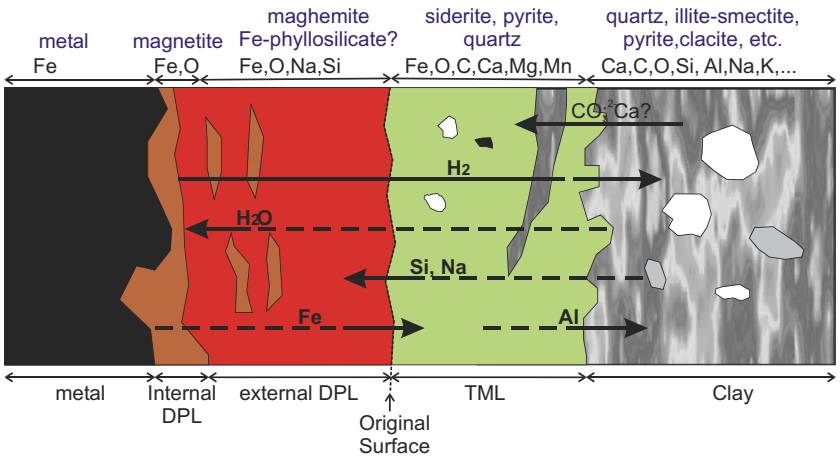

Fig. 13. Outline of elemental transfers at the iron-clay corroded interface in the case of Bure site callovo-Oxfordian argilite. The major elements (in black) and the various major mineral phases (in blue) are indicated above the figure. The morphological units are indicated in the lower part of the sketch (from [18]).

layers as calcium-substituted siderite were the same and the internal magnetite layer was also evidenced. In the case of Bure argilite, a new product was evidenced, which added a new layer/component to the kinetics/diffusion system. It was thus difficult to take the same value for λ.

According to the 'post mortem' analysis [18], the dense product layer was actually composed of two sub-layers: an internal DPL, made of magnetite, and an external DPL apparently made of Fe-phyllosilicates. The iDPL relics found by SEM-EDX inside the eDPL during a closer study of the cross section of the Fe sample suggest the eDPL has grown from the magnetite. This eDPL (Fe-phyllosilicate) was thus created by 'eating' the magnetite (iDPL) by diffusion of Si and Na from the surrounding layer of clay. This observation is definitely relevant with the information collected by *in situ* EIS during the test.

The exact nature of these Fe-phyllosilicates has been investigated and detailed by Schlegel et al. [18], and it appeared the identification was not obvious: stevensite is mentioned, concerning the Fe K-edge EXAFS analyses, the best fit was obtained with a linear combination of 2 types of clay minerals (nontronite, minnesotaite...), but saponite would have been a good candidate as well. Anyway, the most important result was that most neoformation of clay minerals (by diffusion in magnetite) took place in the corrosion layer, not in the transformed clay.

To sum up these considerations, an outline of elemental transfers at the iron-clay corroded interface has been sketched in Fig. 13. The major elements (in black) and the various mineral major phases (in blue) are indicated on top of the figure. The morphological units are indicated in the lower part of the figure.

6. Conclusions

This electrochemical study used *in situ* monitoring as chronopotentiometry and EIS. It was clearly observed that in both clays, the pure iron or the 1050 steel tended to passivate with time, with mainly two steps: formation of a corrosion layer, then limitation of the corrosion kinetics by diffusive phenomena. Post-mortem analyses evidenced the formation of a thin layer of magnetite at the metal interface, then formation of a layer of calcium-substituted siderite in both types of clay. The presence of this siderite has been correlated to a decrease of the corrosion rate in the case of MX80 clay down to 3 μm/year at 90 °C. The case of Bure argilite seemed a bit more complex with the presence of a new corrosion layer in the dense product layer, which grew from the magnetite thanks to Na and Si ions diffusion from the external clay minerals. The formation of such a complex continuous corrosion product layer may also act specifically on the corrosion rate, which tended towards a limit value for long times.

Moreover, it seems that for low alloyed steels in contact with Bure Callovo-Oxfordian clay, the corrosion products had a good affinity for Si. This could be a new dimensioning factor to consider for the degradation scenarios of waste packages under anaerobic deep geological disposal conditions.

Acknowledgements

Authors are grateful to P. Vigier for his assistance in set-up configuration and sample preparation. This work has been supported by ANDRA (French National Agency Responsible for the Management of Radioactive Nuclear Waste) and EDF.

References

[1] ANDRA Public Report, Andra Edts, Chatenay-Malabry, France, 2005.
[2] F.T. Madsen, Clay Min. 33 (1998) 109.
[3] Y. Inagaki, A. Ogata, H. Furuya, K. Idemitsu, in: W.M. Murphy, D.A. Knecht (Eds.), Scientific Basis for Nuclear Waste Management XIX, Ed. Material Research Society, vol. 412, 1996, p. 257.
[4] S. Gin, P. Jollivet, J.-P. Mestre, M. Jullien, C. Pozo, Appl. Geochem. 16 (7–8) (2001) 861.
[5] J. Wilson, D. Savage, J. Cuadros, M. Shibata, K.V. Ragnarsdottir, Geochim. Cosmochim. Acta 70 (2006) 306.
[6] O. Bildstein, L. Trotignon, M. Perronnet, M. Jullien, Phys. Chem. Earth 31 (2006) 618.
[7] D. Guillaume, A. Neaman, M. Cathelineau, R. Mosser-Ruck, C. Peiffert, M. Abdelmoula, J. Dubessy, F. Villieras, N. Michau, Clay Min. 39 (2004) 17.
[8] S. Lantenois, B. Lanson, F. Muller, A. Bauer, M. Jullien, A. Plancon, Clays Clay Min. 53 (2005) 597.
[9] J. Wilson, G. Cressey, B. Cressey, J. Cuadros, K.V. Ragnarsdottir, D. Savage, M. Shibata, Geochim. Cosmochim. Acta 70 (2006) 323.
[10] M. Perronnet, Reactivité des matériaux argileux dans un contexte de corrosion métallique. Application au stockage des déchets radioactifs en site argileux, PhD thesis, Institut National Polytechnique de Lorraine, France, 2004, p. 283.
[11] W. Debruyn, J. Dresselaers, P. H. Vermeiren, J. Kelchtermans, H. Tas, Corrosion of container and infrastructure materials under clay repository conditions, SCK-CEN, Report CEC EUR-13667 EN, 1991, p. 129.
[12] F. Papillon, M. Jullien, C. Bataillon, in: D. Féron, D.D. MacDonald (Eds.), Prediction of theLong Term Corrosion Behaviour inNuclear Waste Systems 36, European Federation of Corrosion Publications, Maney Publishing, UK, 2003, p. 439.
[13] S. Lantenois, Réactivité fer métal/smectites en milieu hydraté à 80 °C, PhD thesis, Université d'Orléans, France, 2003, p. 226.
[14] C. Bataillon, C. Musy, M. Roy, J. Phys. IV 11 (2001) 267.
[15] D. Neff, S. Reguer, L. Bellot-Gurlet, P. Dillmann, R. Bertholon, J. Raman Spectrosc. 35 (2004) 739.
[16] D.S. Dunn, M.B. Bogart, C.S. Brossia, G.A. Cragnolino, Corrosion 56 (2000) 470.
[17] D. Grolimund, M. Senn, M. Trottmann, M. Janousch, I. Bonhoure, A.M. Scheidegger, M. Marcus, Spectrochim. Acta B 59 (2004) 1627.

[18] M.L. Schlegel, C. Bataillon, K. Benhamida, C. Blanc, D. Menut, J.-L. Lacour, Appl. Geochem., accepted for publication.
[19] G. Montes-H, N. Marty, B. Fritz, A. Clement, N. Michau, Appl. Clay Sci. 30 (2005) 181.
[20] E. Sauzeat, D. Guillaume, A. Neaman, J. Dubessy, M. François, C. Pfeiffer, M. Pelletier, R. Ruch, O. Barres, J. Yvon, F. Villéas, M. Cathelineau, Caractérisation minéralogique, cristallographique et texturale de l'argile MX80, Rapport ANDRA No CRP0ENG 01-001, 2001, p. 82.
[21] G. de Combarieu, P. Barboux, Y. Minet, Phys. Chem. Earth 32 (2007) 346.
[22] E. Gaucher, C. Robelin, J.M. Matray, G. Negral, Y. Gros, J.F. Heitz, A. Vinsot, H. Rebours, A. Cassagnabere, A. Bouchet, Phys. Chem. Earth 29 (2004) 55.
[23] P. Vieillard, S. Ramirez, A. Bouchet, A. Cassagnabère, A. Meunier, E. Jacquot, Appl. Geochem. 19 (2004) 1699.
[24] M. Pourbaix, Atlas of Electrochemical Equilibria, Pergamon Press, New-York, 1966.
[25] C. Bataillon, F.A. Martin, M. Roy, Corrosion Monitoring of Carbon Steel in Pasty Clayey Mixture as Function of Temperature, European Federation of Corrosion Publications, Woodhead Publishing, Cambridge, UK, in press.